

# Hyperdimensional Feature Fusion for Interpretable Out-Of-Distribution Detection

Samuel Wilson<sup>1</sup>[0000-0002-3320-3950], Tobias Fischer<sup>1</sup>[0000-0003-2183-017X],  
Niko Sünderhauf<sup>1</sup>[0000-0001-5286-3789], and Feras Dayoub<sup>2</sup>[0000-0002-4234-7374]

<sup>1</sup> Queensland University of Technology <sup>\*</sup>, Brisbane QLD 4000, Australia  
{s202.wilson,tobias.fischer,niko.suenderhauf}@qut.edu.au

<sup>2</sup> Australian Institute for Machine Learning, Adelaide SA 5000, Australia  
feras.dayoub@adelaide.edu.au

**Abstract.** We introduce powerful ideas from Hyperdimensional Computing into the challenging field of Out-of-Distribution (OOD) detection. In contrast to most existing works that perform OOD detection based on only a single layer of a neural network, we use similarity-preserving semi-orthogonal projection matrices to project the feature maps from *multiple* layers into a common vector space. By repeatedly applying the *bundling* operation  $\oplus$ , we create expressive class-specific descriptor vectors for all in-distribution classes. At test time, a simple and efficient cosine similarity calculation between descriptor vectors consistently identifies OOD samples with competitive performance to the current state-of-the-art and minimal computational overhead. By representing visual similarity between inputs and classes as cosine similarity between vectors, HDFS provides a simple method to interpreting its predictions.

## 1 Introduction

Deep Neural Networks can achieve excellent performance on many vision tasks when the distribution of training data closely matches the test data. However, this assumption is often violated during deployment: especially in embodied AI application domains such as robotics and autonomous systems, objects and scenes that were not part of the training data distribution will inevitably be encountered. When confronted with such out-of-distribution (OOD) samples, deep neural networks tend to fail silently, producing overconfident but erroneous predictions [16,48] that can pose severe risks [53]. It is therefore critically important that OOD samples are identified effectively during deployment.

Previous techniques for OOD detection used softmax probabilities [18,28] or distances in logit space [17] to distinguish in-distribution (ID) from OOD samples, making the implicit assumption that the features of a *single* layer in

---

<sup>\*</sup> The authors acknowledge continued support from the Queensland University of Technology (QUT) through the Centre for Robotics. We also thank Peer Neubert from Chemnitz University of Technology for greatly insightful discussions on the topic of Hyperdimensional Computing.

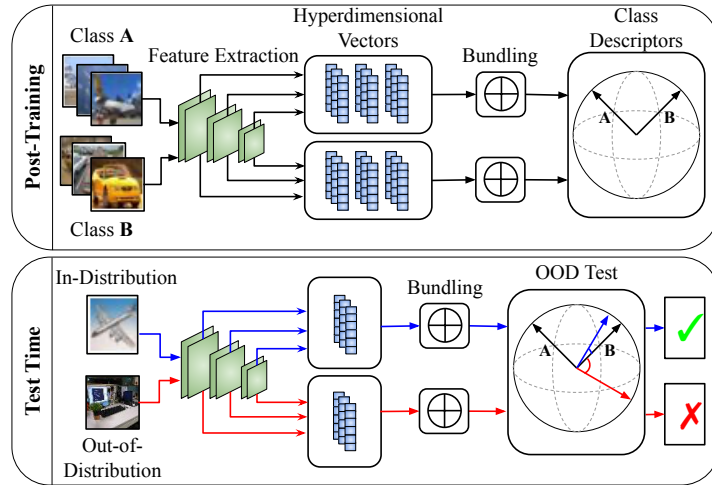


Fig. 1: Illustration of our HDFF OOD detector. **Top:** After training, we extract the feature maps of in-distribution classes from multiple layers of the DNN and project them into a new hyperdimensional space with a similarity-preserving projection matrix. Using the bundling operation  $\oplus$  we create class-specific hyperdimensional descriptor vectors. **Bottom:** During testing, we repeat feature extraction, projection and bundling to obtain a hyperdimensional image descriptor. OOD samples will produce descriptors with a large angular distance to all class descriptors (red vector).

a Deep Neural Network (DNN) contain sufficient information to identify OOD data. However, deeper layers of a DNN can be more sensitive to OOD samples than the softmax probabilities [43], which are often overconfident in the presence of OOD samples [16]. Recent work investigating the utility of multi-scale deep features from a DNN found that modelling ID classes from raw features is difficult without first reducing the number of dimensions [43,27,41] due to the curse of dimensionality [59]. Due to the black box nature of deep networks, generating representations that are both interpretable and useful for OOD detection is hard and as such we see a tendency toward statistics-like methods that only report a single score [49,30,27].

In this paper, we introduce the powerful concepts of similarity-preserving projection, binding and bundling from Hyper Dimensional Computing (HDC) [52] to OOD detection. Figure 1 provides a high-level description of our proposed OOD detector. We project the feature maps from *multiple* layers of a network into a common high-dimensional vector space, using similarity-preserving semi-orthogonal projection matrices. This allows us to effectively *fuse* the information contained in multiple layers: a series of *bundling* operations  $\oplus$  creates a class-specific high-dimensional vector representation for each of the in-distribution classes from the training dataset. During testing, we use the same principles of projection and bundling to obtain a single vector representation for a new input

image. OOD samples can then be efficiently identified through cosine similarity operations with the class-specific representations.

Our Hyperdimensional Feature Fusion (HDFF) approach relies on the pseudo-random nature of its projection matrices and the similarity-preserving properties of the bundling operation  $\oplus$  to effectively fuse information contained in the feature maps across multiple layers in a deep network. HDFF avoids the difficulties of estimating densities in high-dimensional spaces [43,27], removes the limitation of relying on a single layer [18,17], does not require to select informative layers based on example OOD data [21,56,30], and does not necessarily rely on expensive sampling techniques (such as ensembles [25] or Monte Carlo Dropout [10]) to identify OOD samples. HDFF can be applied to a trained network and does not require re-training or fine-tuning. Our HDFF detector competes with or exceeds state-of-the-art performance for OOD detection in conjunction with networks trained with standard cross-entropy loss or more sophisticated logit space shaping approaches [57].

In summary, our contributions are the following:

1. We propose a novel OOD detector based on the principles of Hyperdimensional Computing that is competitive with state-of-the-art OOD detectors with the benefit of interpretability.
2. We show that fusing features from multiple layers is critical for general OOD detection performance, as different layers vary in sensitivity to different OOD data, but fusion results in OOD performance that is approximately on par or even better than the best single layer.
3. We show that the angles between HDFF vectors can be interpreted as visual similarity between inputs, allowing for failure diagnosis.

## 2 Related Work

Out-of-distribution (OOD) detection has been addressed in the context of image classification [28,30,57,18] and semantic segmentation [17,9,1,2] with a diverse set of solutions to each of the problems. In this section, we highlight overarching concepts and most relevant contributions in three areas: i) Many approaches try to extrapolate the properties of the distribution of OOD data by utilising a small subset of the data to fine-tune on. ii) When this information is unavailable (OOD agnostic), distances or densities in the softmax probabilities and logit spaces are used. iii) Comparatively few bodies of work exist that use multiple feature maps for OOD detection.

**OOD Fine-tuning** Some prior work [47,21,56,30,28,9,1] requires the availability of an OOD dataset to train or fine-tune the network or adjust the OOD detection process. However, such approaches are problematic. By definition, the OOD dataset has to always be incomplete: during deployment, samples that do not match the assumptions embedded in the OOD dataset can still be encountered, leaving such methods exposed to high OOD risk. In contrast, we do not require prior knowledge about the characteristics of OOD data.

**OOD Agnostic** Most approaches that do not rely on the availability of OOD data during training or validation analyse the model outputs to identify OOD

data during deployment. Early work [18] showed the maximum of a model’s softmax output to be a good baseline. Expanding on this idea, [17] proposed using the maximum of the unnormalised output logits. Additional methods focus on extracting more information from the outputs [40] or learning calibrated confidence estimates [8,26]. Model averaging techniques such as Deep Ensembles [25], Monte Carlo (MC) Dropout [10,17] and SWA-G [31,57] often improve the OOD detection performance. Training networks with specialised losses that impose a beneficial structure on the feature space has been growing in popularity [33,57,34]. E.g. the recent 1D Subspaces [57] OOD estimator encourages the network to learn orthogonal features in the layer before the logits. The approaches discussed above attempt OOD detection based on only a *single* layer in the network. In contrast, we show that utilising *multiple* layers is beneficial for OOD detection.

**Multi-Feature OOD Detection** Newer approaches incorporate and analyse multi-scale feature maps extracted from a DNN to detect OOD samples. The use of feature maps and additional information extracted from a network has been shown to set a new state-of-the-art in OOD segmentation [9,1] when used as input to an auxiliary OOD detection network. The requirement on an auxiliary network necessarily entails training on OOD data in the OOD detection task, but in the related field of online performance monitoring we see similar methods demonstrate failure case detection without knowledge of the types of failures to be encountered [45,46]. Avoiding these problems altogether, recent works have tried to model in-distribution classes without an auxiliary network [43,27,41]. However, the curse of dimensionality requires these methods to rely on PCA reductions [43,27] or random projections [41], losing information from the feature maps. By contrast, we use techniques from Hyperdimensional Computing to model our in-distribution data without the need for an auxiliary network or reducing the feature maps. We seek to build upon evidence in the literature [43,49,29] that multi-scale features benefit OOD detection performance by introducing the added benefits of interpretability with powerful OOD techniques.

### 3 Hyperdimensional Computing

Hyperdimensional Computing (HDC), also known as Vector Symbolic Architectures, is the field of computation with vectors in hyperdimensional, very large, spaces. HDC techniques leverage the large amount of expressive power in the hyperdimensional (HD) space to model associations between data points using redundant HD vector encodings. Redundant means that in spaces of  $10^4$  dimensionality it can be seen that two random vectors are almost guaranteed to be within 5 degrees of orthogonal [51] known as *quasi-orthogonality*. The associations between data points are represented as vectors, and the set of the representative vectors is known as the *associative memory* [13]. Construction of the associative memory is done through the structured combination of HD vectors using a set of standard operations. For our application we are primarily interested in the *bundling*  $\oplus$  and *binding*  $\otimes$  operation for combining feature vec-

tors, and the *encoding* operation for projecting low dimensional representations into our target HD space.

**Bundling** The bundling  $\oplus$  operation is used to store a representation of multiple input vectors that retains similarity to all of the input vectors [42]. Concretely, given random vectors  $\mathbf{a}$ ,  $\mathbf{b}$  and  $\mathbf{c}$ , the vector  $\mathbf{a}$  will be similar to the bundles  $\mathbf{a} \oplus \mathbf{b}$ ,  $\mathbf{a} \oplus \mathbf{c}$  and  $\mathbf{a} \oplus \mathbf{b} \oplus \mathbf{c}$ , although in the final case it will be less similar as the bundled vector needs to be similar to all 3 input vectors. Typically, the bundling operation is implemented as element-wise addition with some form of normalisation to the required space for the architecture [51]. Normalisation steps that are commonly seen are normalisation to a magnitude of one [14,11] or cutting/thresholding to a range of desired values [12]. Without normalisation, the bundling operation is commutative and associative; when normalisation steps are added the associative aspect of the operation is approximate,  $(\mathbf{a} \oplus \mathbf{b}) \oplus \mathbf{c} \approx \mathbf{a} \oplus (\mathbf{b} \oplus \mathbf{c})$  [51].

**Binding** The binding  $\otimes$  operation is used to combine a set of vectors into one representation that is dissimilar to all of the input vectors [42]. Given the quasi-orthogonality property of HD spaces, this entails that in all likelihood, the binding operation will generate a vector orthogonal to all of the input vectors in the cosine similarity space. The second core trait of the binding operation is that it approximately preserves the similarity of two vectors before and after binding if they are bound to the same target vector. More precisely, for a set of vectors in the same hyperdimensional space  $\mathbf{a}$ ,  $\mathbf{b}$  and  $\mathbf{c}$ , that  $sim(\mathbf{a}, \mathbf{b}) \approx sim(\mathbf{a} \otimes \mathbf{c}, \mathbf{b} \otimes \mathbf{c})$ .

**Encoding** The format of the original data will not always be in the hyperdimensional space that is required. Encoding addresses this by projecting each data point from the original space into the new HD space. The selection of data encoding into a HD space depends on the type of the original data [44,19]. An important principle of encoding is that distances in the input are preserved in the output [19], much like the binding operation. Examples of encoding include multiplication with a projection matrix [35], fractional binding [23] that preserves real numbered differences, or the encoding proposed in [19] that preserves similarities of vectors over time and spatial coordinates.

We provided only a brief introduction to HDC, for more in-depth discussions and comparisons between known architectures we encourage the reader to consider [51,38,22].

## 4 Hyperdimensional Feature Fusion

We propose Hyperdimensional Feature Fusion (HDFF), a novel OOD detection method that applies the HDC concepts of Encoding and Bundling to the features from *multiple* layers in a deep neural network, without requiring re-training or any prior knowledge of the OOD data. Our core idea is to project the feature maps from multiple layers into a common vector space, using similarity-preserving semi-orthogonal projection matrices. Through a series of bundling operations, we create a class-specific vector-shaped representation for each of the classes in the training dataset. During deployment, we repeat the projection

and bundling steps for a new input image, and use the cosine similarity to the class representatives to identify OOD samples. We provide pseudo code to assist with describing our HDFF detector in Algorithm 1.

**Preliminaries** From a pretrained network  $f$ , we can extract feature maps  $\mathbf{m}_l$  from different layers  $l \in \{1, \dots, L\}$  in the the network. We apply a pooling operation across the spatial dimensions to reduce the tensor-shaped (height  $\times$  width  $\times$  channels) feature maps to vector representations  $\mathbf{v}_l$  of length (channels) for each layer; we ablate the effects of different pooling in the Appendix. Since the feature maps of different layers have a different number of channels  $c_l$ , we need to project the vectors  $\mathbf{v}_l$  into a common  $m$ -dimensional vector space  $\mathbb{R}^m$  in order to combine them. Conventional sizes for HD spaces range around  $10^3$  -  $10^4$  [39,35,19], meaning that typically our HD space will be much larger than our original space  $m \gg c$ .

**Feature Encoding** Any  $m \times c$  matrix  $\mathbf{P}$  projects a  $c$ -dimensional vector  $\mathbf{v}$  into a  $m$ -dimensional space by left-multiplying:  $\mathbf{P}\mathbf{v}$ . However, preserving the cosine similarity of the projected vectors is a crucial consideration for our application in OOD detection. We therefore impose that the projection matrices  $\mathbf{P}_l$  preserve the inner product of any two vectors  $\mathbf{a}$  and  $\mathbf{b}$  in their original and their projected vector spaces. Formally, this means that

$$(\mathbf{P} \cdot \mathbf{a})^\top \cdot (\mathbf{P} \cdot \mathbf{b}) = \mathbf{a}^\top \cdot \mathbf{b} \quad (1)$$

$$\mathbf{a}^\top \cdot \mathbf{P}^\top \cdot \mathbf{P} \cdot \mathbf{b} = \mathbf{a}^\top \cdot \mathbf{b} \quad (2)$$

Above condition is satisfied by any matrix that fulfils the requirement  $\mathbf{P}^\top \mathbf{P} = \mathbf{I}$ , which is the defining property of a semi-orthogonal matrix. Using the approach of [50], we therefore create a unique, pseudo-random, semi-orthogonal projection matrix  $\mathbf{P}_l$  for each of the considered layers  $l$ . These project the feature vectors  $\mathbf{v}_l$  into a common  $m$ -dimensional vector space:

$$\mathbf{h}_l = \mathbf{P}_l \mathbf{v}_l \quad \text{so that } \mathbf{h}_l \in \mathbb{R}^m \quad \forall l \in \{1, \dots, L\} \quad (3)$$

**Feature Bundling** Following the previous steps, we obtain a set of  $L$  high-dimensional vectors  $\mathbf{h}_l^{(i)}$  for an input image  $\mathbf{x}^{(i)}$ . Since all  $\mathbf{h}_l^{(i)}$  are elements of the same vector space, we can use the bundling operation  $\oplus$  to combine them into a single vector  $\mathbf{y}^{(i)}$  that serves as an expressive descriptor for the input image  $\mathbf{x}^{(i)}$ :

$$\mathbf{y}^{(i)} = \bigoplus_{l=1}^L \mathbf{h}_l^{(i)} = \bigoplus_{l=1}^L \mathbf{P}_l \cdot \mathbf{v}_l^{(i)} \quad (4)$$

As explained in Section 3, the resulting vector  $\mathbf{y}^{(i)}$  will be cosine-similar to all contributing vectors  $\mathbf{h}_l^{(i)}$ , but dissimilar to vectors from  $\mathbb{R}^m$  that were not part of the bundle. Essentially,  $\mathbf{y}^{(i)}$  provides a summary of the feature vectors  $\mathbf{v}_l^{(i)}$  of the entire network for a single image  $\mathbf{x}^{(i)}$ .

By bundling the descriptors of all images from the training set belonging to class  $c$ , we obtain a class-specific descriptor  $\mathbf{d}_c$ :

$$\mathbf{d}_c = \bigoplus_{j \in \mathbb{I}_c} \mathbf{y}^{(j)} \quad (5)$$

---

**Algorithm 1** Computation of the model-wise class descriptors and ensemble descriptor vectors from training set.

---

**Inputs:** Set of images from the training set  $x^{\{1, \dots, I\}}$  with corresponding labels  $j^{\{1, \dots, I\}}$ . Set of models in an ensemble  $f_{\{1, \dots, E\}}$  that produces a set of feature maps  $\mathbf{m}_{\{1, \dots, L\}}$  given an input  $x^{(i)}$ .

**Outputs:** Set of class descriptor vectors per input model  $d_{\{1, \dots, c\}}^{(e)}$  and a set of ensemble class descriptor vectors  $d^*$

```

for  $e \in \{1, \dots, E\}$  do
  for  $i \in \{1, \dots, I\}$  do
     $m_{\{1, \dots, L\}}^{(i)} \leftarrow f_e(x^{(i)})$ 
    for  $l \in \{1, \dots, L\}$  do
       $v_l^{(i)} \leftarrow \text{Pool}(m_l^{(i)})$ 
       $h_l^{(i)} \leftarrow P_l \cdot v_l^{(i)}$ 
    end for
     $y^{(i)} \leftarrow h_1^{(i)} \oplus h_2^{(i)} \oplus \dots \oplus h_L^{(i)}$ 
     $d_{j^{(i)}}^{(e)} \leftarrow d_{j^{(i)}}^{(e)} \oplus y^{(i)}$ 
  end for
end for
 $d^* \leftarrow (d^{(1)} \otimes z^{(1)}) \oplus \dots \oplus (d^{(E)} \otimes z^{(E)})$ 

```

---

where  $\mathbb{I}_c$  denotes the set of indices of the training images belonging to class  $c$ .

As discussed in Section 3, the bundling operation  $\oplus$  can be implemented in various ways. We implement  $\oplus$  to be an element-wise sum, without truncation.

**Out-of-Distribution Detection** During testing or deployment, an image  $\mathbf{x}$  can be identified as OOD by obtaining its image descriptor  $\mathbf{y}$  according to (4), and calculating the cosine similarity to each of the class-specific descriptors  $\mathbf{d}_c$ . Let  $\theta$  be the angle to the class descriptor  $\mathbf{d}_c$  that is most similar to  $\mathbf{y}$

$$\theta = \min_c \cos^{-1} \left( \frac{\mathbf{y}^\top \mathbf{d}_c}{\|\mathbf{y}\| \cdot \|\mathbf{d}_c\|} \right), \quad c \in \{1, \dots, C\}, \quad (6)$$

The input  $\mathbf{x}$  is then treated as OOD if  $\theta$  is bigger than a threshold:  $\theta > \theta^*$ .

**Ensembling** While HDFE does not rely on ensembling, we briefly show that our method is amenable to ensembling to further boost performance (however at the cost of added compute). When using a set of pretrained networks  $f_e$  in an ensemble  $e \in \{1, \dots, E\}$  we collect inputs from all models and fuse them into singular image and class descriptors  $\mathbf{y}_*$  and  $\mathbf{d}^*$  respectively. For each model  $f_{\{1, \dots, E\}}$  the same process using equations (4) and (5) is used to compute the set of class descriptors for each model in the ensemble  $\mathbf{d}^{\{1, \dots, E\}}$ . To ensure that each class descriptor is sufficiently distinct from all other descriptors, a set of random hyperdimensional vectors  $\mathbf{z}^{(e)}$  are generated and bound  $\otimes$  to the class descriptor. By bundling the bound class descriptors, we obtain the ensemble class descriptor  $\mathbf{d}^*$ :

$$\mathbf{d}^* = \bigoplus_{e=1}^E \mathbf{d}^{(e)} \otimes \mathbf{z}^{(e)} \quad (7)$$

When new input samples arrive  $\mathbf{y}_*$  is computed according to (7) by substituting  $\mathbf{d}$  for  $\mathbf{y}$ . OOD detection is done according to (6) using  $\mathbf{d}^*$  and  $\mathbf{y}_*$ .

## 5 Experiments

We conduct a series of experiments to demonstrate the efficacy of Hyperdimensional Feature Fusion for OOD detection. We compare HDFS to the current state-of-the-art in the typical far-OOD settings, where the distributions of the ID and OOD are very dissimilar (e.g. CIFAR10  $\rightarrow$  SVHN), and the more challenging near-OOD where the ID and OOD datasets are drawn from similar distributions (e.g. CIFAR10  $\rightarrow$  CIFAR100). Further, we report the results of some critical ablation studies, in particular, we identify which layers are most sensitive to OOD data and how sensitive HDFS is to the decision parameter  $\theta^*$  during deployment.

### 5.1 Experimental Setup

**Datasets** For our comparisons to existing OOD detectors we use a wide array of popular datasets composed from multiple recent state-of-the-art OOD detectors. We construct our evaluation suite as the combination of datasets from [28,49,29]. For our comparison to existing OOD detectors, we use the popular dataset splits for near- and far-OOD detection using CIFAR10 and CIFAR100 [24] as the ID datasets. For our ID sets, we use the 50,000 training examples for training and computation of the class bundles, whilst the 10,000 testing images are used as our unseen ID data. For the near-OOD configurations, the test set of whichever CIFAR dataset is not being used for training will be used as the OOD set. For the far-OOD detection settings, we use a suite of benchmarks: iSUN, TinyImageNet [6] (cropped and resized: TINc and TINr), LSUN [55] (cropped and resized: LSUNc and LSUNr)<sup>3</sup>, SVHN [37], MNIST [7], KMNIST [4], FashionMNIST [54], DTD [3] and STL10 [5].

**Evaluation Metrics** We consider the standard metrics [57,49] for our comparison to existing OOD literature. **AUROC:** The Area Under The Receiver Operating Characteristic curve corresponds to the area under the ROC curve with true positive rate (TPR) on the y-axis and false positive rate (FPR) on the x-axis. AUROC can be interpreted as the probability that an OOD sample will be given a higher score than an ID sample [17]. **FPR95:** The FPR95 metric reports the FPR at a critical threshold which achieves a minimum of 95% in TPR. **Detection Error:** Detection Error indicates the minimum misclassification probability with respect to the critical threshold. **F1:** F1-score corresponds to the harmonic mean of precision and recall. We make use of F1-score to evaluate the general binarisation performance in our ablations. In the interests of brevity, we only evaluate using the AUROC metric for our evaluations. We provide additional evaluations with FPR95 and Detection Error in the Appendix.

<sup>3</sup> Download links for OOD datasets can be found in the following repository: <https://github.com/facebookresearch/odin>

ID set	OOD set	HDFF (Ours)	HDFF† (Ours)	Gram [49]	HDFF‡ (Ours)	HDFF†‡ (Ours)	Gram‡ [49]	Spectral‡ [57]	DDU [36]	MOOD [29]
CIFAR10	iSun	99.2	99.3	<b>99.9</b>	<b>99.9</b>	<b>99.9</b>	<b>99.9</b>	-	-	92.96
	TINc	98.3	98.4	99.4	<i>99.7</i>	<b>99.8</b>	99.5	98.1	91.07*	-
	TINr	99.2	99.4	<i>99.8</i>	<i>99.8</i>	<b>99.9</b>	<i>99.8</i>	98.5	91.07*	-
	LSUNc	96.2	96.8	98.1	99.1	<b>99.6</b>	98.6	<i>99.4</i>	-	99.23
	LSUNr	99.2	99.4	<b>99.9</b>	<b>99.9</b>	<b>99.9</b>	<b>99.9</b>	99.3	-	93.25
	SVHN	99.4	<i>99.5</i>	99.4	99.2	<b>99.6</b>	<i>99.5</i>	-	97.86	96.49
	MNIST	99.6	99.7	<i>99.97</i>	99.3	99.3	<b>99.98</b>	-	-	99.79
	KMNIST	99	99.1	<i>99.98</i>	99.3	99.5	<b>99.99</b>	-	-	99.86
	FMNIST	98.7	99.1	99.8	99.3	99.5	<b>99.9</b>	-	-	<b>99.91</b>
	DTD	94.5	94.8	<i>98.2</i>	97.3	98.1	<b>98.4</b>	-	-	83.32
	STL10	59.8	59.9	<b>88.3</b>	69.6	70.5	<i>87.7</i>	-	-	61.31
	CIFAR100	75.4	75.8	79.4	90.7	<b>92.7</b>	78.7	-	<i>91.34</i>	-
CIFAR100	iSun	95.8	95.8	<i>98.8</i>	94.6	97.6	<b>99.6</b>	-	-	77.84
	TINc	92.7	93.2	<i>98.2</i>	93.7	95.1	<b>98.7</b>	88.6	83.13*	-
	TINr	96.1	96	<i>98.5</i>	94.1	97	<b>99.1</b>	93.7	83.13*	-
	LSUNc	86.5	88.8	96	91.8	92.2	<b>97.9</b>	93.8	-	<i>96.83</i>
	LSUNr	95.4	95.4	<i>99.3</i>	95.1	97.9	<b>99.6</b>	95.7	-	77.6
	SVHN	99.2	<i>99.4</i>	99	92.8	96.2	<b>99.6</b>	-	87.53	85.88
	MNIST	99.8	99.8	<i>99.9</i>	96.7	99.1	<b>100</b>	-	-	91.34
	KMNIST	99.5	99.6	<i>99.99</i>	98.4	99.4	<b>100</b>	-	-	97.17
	FMNIST	98.3	98.4	<b>99.4</b>	97.8	99.1	<b>99.4</b>	-	-	99.11
	DTD	92.9	93.5	<b>97.5</b>	86.2	90.4	<i>97.4</i>	-	-	71.69
	STL10	66.5	68.6	<i>89.5</i>	79.9	81.1	<b>91.7</b>	-	-	77.58
	CIFAR10	65.9	68.2	74.2	78.1	<i>79.7</i>	<b>80.8</b>	-	-	-
<b>Average</b>		92.0	92.4	<i>96.4</i>	93.8	95.1	<b>96.9</b>	95.9	88.6	89.0

Table 1: OOD detection comparison against state-of-the-art OOD detectors. Comparison metric is AUROC, higher is better. **Best** results for a data set are shown in **blue and bold**, *second* best results are shown in *green and italics*. A dagger† is used when HDFF is ensemble; there are always 5 models in the ensemble. A double dagger‡ is used to distinguish methods that are trained with the 1D Subs [57] training methodology. For DDU [36], published TIN results that are unclear if they apply to crop or resize are marked with \*. Gram [49] and HDFF outperform all other OOD detectors; however Gram is not interpretable.

**Baselines** For the sake of conciseness, we do not evaluate against standard OOD baselines (i.e. softmax [18]) and instead compare HDFF directly to four recent state-of-the-art OOD detectors. Specifically, we evaluate against: 1D Subspaces (1D Subs) training with spectral discrepancy (Spectral) detector [57], Deep Deterministic Uncertainty [36] (DDU), Gramian Matrices [49] (Gram) and Multi-level Out-of-distribution Detection [29] (MOOD). Gram is the most similar method to ours, so in the interest of fairest comparison, we extend upon the public code available to adapt their approach to more models and datasets than the original. For all other detectors, we use the published results. We note that the published results for the Spectral Discrepancy [57] detector are achieved after collecting 50 Monte Carlo samples with SWA-G [32].

**Implementation** We follow the evaluation procedure defined in [57,28], implementing the standard WideResNet [58] network with a depth of 28 and a width of 10. For the evaluation, we train this network with the standard cross-

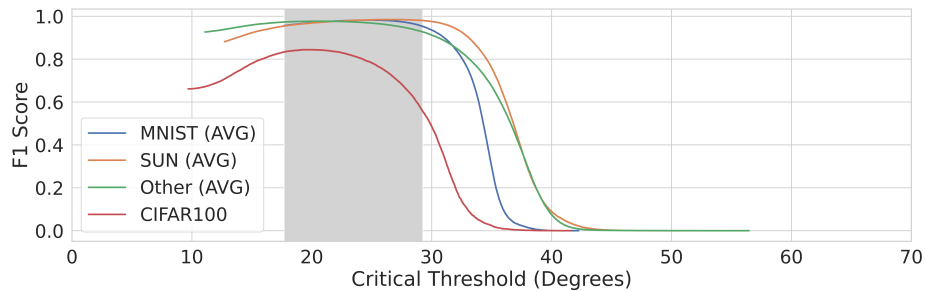


Fig. 2: F1-score for binarisation at different critical values of angular distance to closest class descriptor. The model used is the 1D Subs trained WRN28-10. The grey region corresponds to binarisations that would produce a result within 5% of the maximum F1-score achieved for all far-OOD datasets. To avoid clutter, far-OOD datasets have been grouped: i) MNIST (AVG) contains KMNIST, MNIST and FashionMNIST. ii) SUN (AVG) contains iSUN, LSUNr and LSUNc. iii) Other (AVG) contains all other far-OOD datasets. Just as one would expect, the near-OOD task (CIFAR100) leads to significantly lower thresholds compared to all far-OOD tasks.

entropy loss, and a slightly modified version of the 1D Subs training methodology from [57], exact details of our modifications can be found in the Appendix. As both HDFF and Gram [49] are capable of being added onto any pretrained network, each will be evaluated under both training methodologies. All compared methods, excluding MOOD [29], use the WideResNet [58] network with the same depth and width parameters. Additional evaluations of HDFF and Gram on ResNet34 [15] and DenseNet3 [20] are provided in the Appendix.

When applying HDFF and Gram to the networks we attempt to faithfully recreate the hooks used on the ResNet34 architecture for the WideResNet model. Specifically, features are recorded from the outputs of almost all of the following modules within the network: Conv2d, ReLU, BasicBlock, NetworkBlock and shortcut connections. In total, there are 76 features extracted per sample and hence the same number of semi-orthogonal projection matrices  $\mathbf{P}$  are generated for HDFF.

Unless otherwise stated, we operate in a hyperdimensional space of  $10^4$  dimensions, we ablate this hyperparameter in the Appendix. Before projecting feature maps into the hyperdimensional space as per (5), we apply mean-centering by subtracting the layer-wise mean activations (obtained from the training set) from all  $\mathbf{m}_l$ . For pooling we apply max pooling over the spatial dimensions to reduce our feature maps  $\mathbf{m}_l$  to a vector, we ablate the effect of this choice in the Appendix.

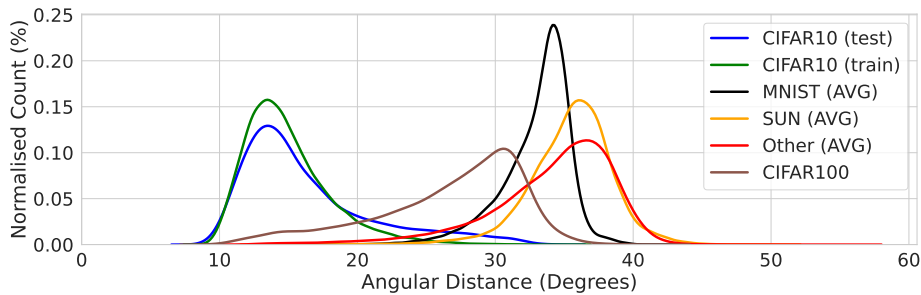


Fig. 3: KDE estimate of separation between ID and OOD sets based on minimum angular distance to closest class representative in the CIFAR10 setting. To avoid clutter, far-OOD datasets have been grouped: i) MNIST (AVG) contains KMNIST, MNIST and FashionMNIST. ii) SUN (AVG) contains iSUN, LSUNr and LSUNc. iii) Other (AVG) contains all other far-OOD datasets. Overlap between the test and OOD distributions can be considered erroneous samples.

## 5.2 Results and Discussion

Table 1 compares the results of our HDFF OOD detector with the AUROC metric to all other methods under both near- and far-OOD settings. The first finding from inspecting Table 1 is that Gram [49] consistently provides strong performance in most settings, which is a positive finding for HDFF as it indicates that a powerful ID representations can be captured from the features the HDFF is using. Further, we observe that in the settings with CIFAR10 as ID, performance gaps between (HDFF, Gram) and (HDFF $\ddagger$ , Gram $\ddagger$ ) are small in most cases, rarely differing by more than 1-2%. This demonstrates that our approach performs as well as, or better than, the state-of-the-art, while having the added benefit of being easily interpretable. HDFF performs considerably better in the near-OOD setting with CIFAR10 as ID set and CIFAR100 as OOD set (AUROC of 92.7 compared to 79.4 of Gram).

## 5.3 Critical Threshold Ablation

During deployment, it is often more useful if an OOD detector produces a binarisation of ID vs OOD rather than a raw OOD estimate; the grey regions in Figure 2 show a range of critical thresholds that will produce performance reasonably close to optimal in this setting. Specifically, the grey region in Figure 2 shows a region of confidence where any critical value would produce an F1-score within 5% of the maximum value achieved on each far-OOD dataset, an approximate standard of reasonable performance. The near-OOD detection task is plotted but does not contribute towards the definition of the grey region due to the severe differences between the near- and far-OOD tasks. As we can see, a large region of critical values around the range of 18-29 degrees will result in generally good performance for far-OOD detection.

#### 5.4 Which Layers Are Most Sensitive To OOD Data?

Figure 4 demonstrates the effectiveness of individual layers when they are used in isolation for OOD detection based on our HDFF OOD estimator. For this ablation, we explicitly change the hook function to only collect features from the outputs of the 12 BasicBlocks and only consider the TIN and LSUN datasets for simplicity. We see in both ID settings that earlier features in the network appear to be less reliable at detecting OOD samples. This trend is particularly obvious in the CIFAR10 setting where a clear trend upwards as the layer number increases is clear. In the CIFAR100 setting we see that this trend is still present, but weaker, primarily due to the outlier of LSUNc which only has high performance on layers 9 and 12. This observation confirms suggestions in prior works that shallow layers in a DNN are unable to detect OOD data [43].

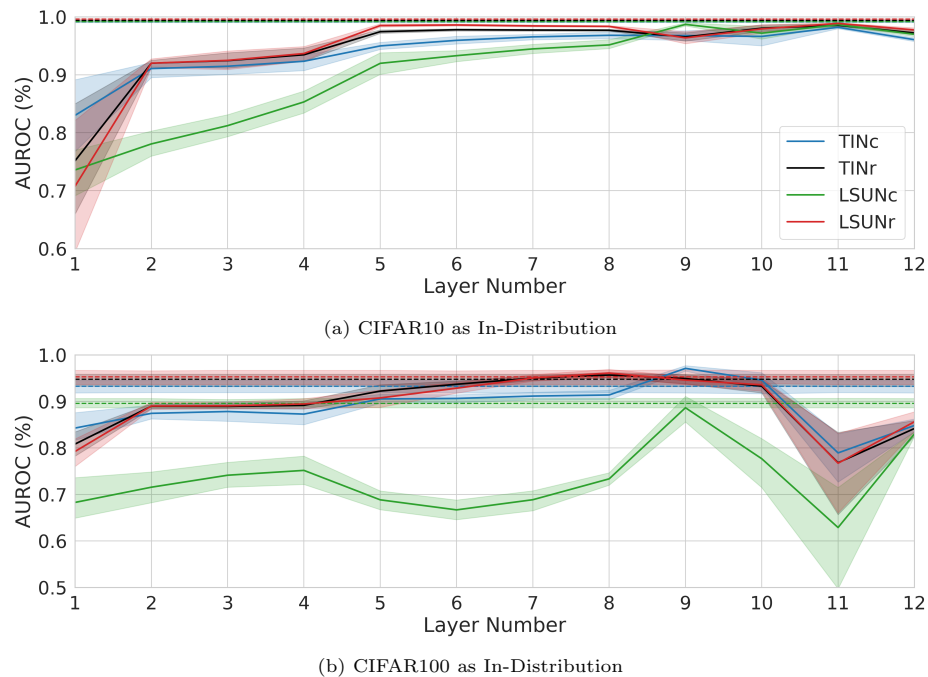


Fig. 4: Comparison of effectiveness for OOD detection of each layer individually with the AUROC measure. Mean and 95% confidence interval over 5 randomly initialised models trained with the 1D Subspaces methodology. Dotted lines correspond to the results attained by the fusion of all 12 BasicBlocks. Performance of individual layers shows a trend toward later layers being more effective at detecting OOD data, with the trend being much stronger in CIFAR10. The fusion of feature maps from across the network provides good general performance across all datasets and does not require calibration on OOD data to set.

The dotted lines, and related 95% confidence shaded area, for each dataset correspond to the fusion of information from all layers; we consider these lines the best that can be reasonably achieved within the bounds of the OOD task. Firstly, in the CIFAR10 setting in Figure 4a we observe that no single individual layer is able to detect the OOD data as well as the fusion of all feature maps. Whilst in the CIFAR100 setting in Figure 4b, we see that the previous observation is sometimes violated, however, this does not indicate a failure of the fusion of feature maps. Critically, we note two points in favour of the fusion of features: (1) without OOD data the optimal layer combination for a given data set is unknown, and (2) the optimal layer combination is not consistent between ID and OOD data configurations. To summarise, note that if there is no access to OOD data at training time to determine which layer(s) are the best then the fusion of feature maps from across the network often provides the best performance or a close approximation. We provide extra ablations against other metrics in the Appendix.

### 5.5 Interpretable OOD

Since HDFF uses similarity preserving projections, in effect, the angular distance represents the differences between raw features. Since the features are extracted from a deep CNN we can consider the angular distance between any two vectors to be a proxy for their visual dissimilarity. This definition leads to intuitive understandings of how HDFF behaves and identifying failure cases; we discuss these points here.

Using our definition, since HDFF separates based on visual similarity, we can infer that failures in OOD detection are due either to ID samples being visually dissimilar to the training set or OOD samples are as similar, if not more so, to the training set than the ID samples. To aid in understanding this, Figure 3 visualises the differences in distributions of angular distance between the ID and OOD datasets in the CIFAR10 ID setting through a KDE estimate (for smoothing) over binned angular distances on the HDFF (1D Subs.) model. The area of overlap between the test set and any OOD set can be considered as erroneous detection. Inspecting Figure 3, we observe that, in the far-OOD settings, errors due to dissimilar ID samples are more likely to appear due to the distributional shift between the training and testing distributions, false positives. By contrast, in the near-OOD detection task we see that a significant number of errors are due to OOD samples appearing very similar to ID samples, false negatives.

We investigate if our hypotheses and definitions hold by taking samples from the CIFAR10 ID test set, CIFAR100 near-OOD set and the TinyImageNet-Crop far-OOD set. Figure 5 demonstrates HDFF separating input samples based on the angle to the nearest class descriptor vector, in this case, the CIFAR10 truck class. Consistent with angular distance corresponding to visual similarity, we observe in Figure 5 that images that are  $< 15^\circ$  from the class descriptor vector appear visually very similar with no far-OOD samples occupying this range. In the range of  $15 - 30^\circ$  we observe that samples from all datasets still have

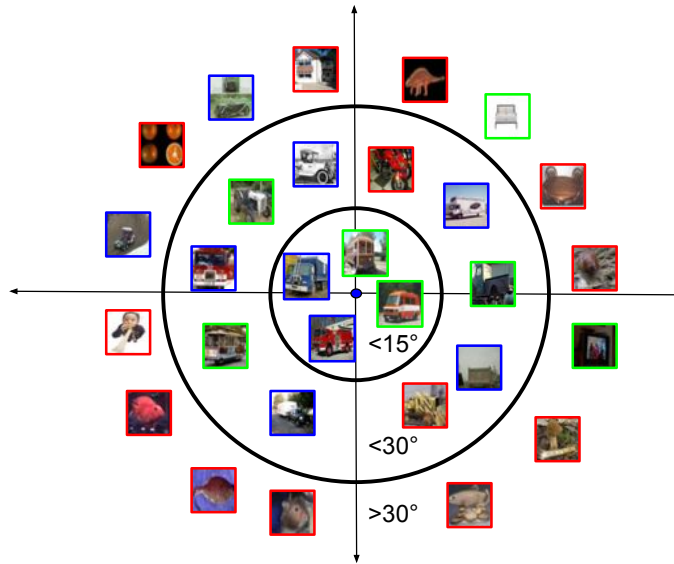


Fig. 5: Sample images from ID (CIFAR10), near-OOD (CIFAR100) and far-OOD (TINc) datasets with their approximate distance to the nearest class descriptor vector, corresponding to the CIFAR10 ID truck class. Images with a blue border are drawn from the ID dataset, green images are drawn from the near-OOD set and red images are drawn from the far-OOD set. Distances to the class bundle (centre blue dot) can be approximately inferred from which circle the sample is encapsulated by.

vehicle-like appearance, but whether or not these accurately represent a truck is debatable; this region is still predominantly populated by ID and near-OOD samples. Once outside the  $30^\circ$  ring, we see that the overwhelming majority of samples do not appear vehicle-like with very few ID samples in this region having the truck visually obscured; this region is dominated by far-OOD samples.

## 6 Conclusion

This paper introduced the powerful ideas from hyperdimensional computing into the important task of OOD detection. We investigate the sensitivity of individual layers to OOD data and find that the fusion of feature maps provides the best general performance with no requirements for OOD data to fine-tune on. We perform competitively with state-of-the-art OOD detection methods with the added benefit of interpretability, allowing for failure diagnosis and alleviating the black box nature of deep networks. In this paper, we utilised the simple but powerful element-wise addition for bundling, however, this is one of potentially many applications of HDC to DNNs, opening new future research directions.

## A Additional Evaluation

As described in the main paper, we provide additional evaluations against extra metrics and network architectures.

### A.1 Additional Metrics

Tables 2 and 3 complete the evaluation from our main paper against the current state-of-the-art against the FPR95 and Detection Error metrics respectively. Note that Table 2 does not include DDU [36] and Table 3 does not include DDU or MOOD [29] as no published results against the relevant metrics exist. Across the board, Tables 2 and 3 reflect the results from the AUROC evaluation in the main paper HDFF and Gram [49] outperforming the other state-of-the-art comparison methods. Consistent with the results from the main paper, we see that the performance gap between HDFF and Gram is relatively minor whilst both improve upon the current state-of-the-art. Overall, the original evaluation against the AUROC metric provides an accurate assessment of the relative performance of the compared methods, with Tables 2 and 3 reinforcing the findings from the original submission.

### A.2 Additional Model Architectures

Table 4 compares the performance of HDFF and Gram [49] on additional model architectures defined by [49] under the AUROC metric. Under the CIFAR100 as ID setting, we observe that HDFF performs better when applied to the DenseNet architecture for the far-OOD settings, but for the more challenging STL10 and CIFAR10 datasets we see a significant performance drop. A similar, but less obvious performance drop is present on the same benchmarks for the CIFAR10 as ID setting. This observation suggests that some network architectures are better at detecting different types of OOD data. Future work into OOD detection could investigate the sensitivity of differing network architectures to specific types of OOD data.

## B Interpretability Extension

### B.1 Comparative Method Interpretability

We consider the interpretability of the compared methods with respect to HDFF as they are the current state-of-the-art in OOD detection.

**HDFF** We start with the benefits of our HDFF detector first. We note that when evaluated under the standard benchmarks and metrics, HDFF is a strong performer for OOD detection, outperforming many state-of-the-art estimators. Additionally, by representing classes and input samples as vectors we introduce the powerful interpretation of angular distance corresponding to visual dissimilarity.

ID set	OOD set	HDFF (Ours)	HDFF <sup>†</sup> (Ours)	Gram [49]	HDFF <sup>‡</sup> (Ours)	HDFF <sup>†‡</sup> (Ours)	Gram <sup>‡</sup> [49]	Spectral <sup>‡</sup> [57]	MOOD [29]
CIFAR10	iSun	3.3	2.68	0.55	0.46	0.24	0.52	-	38.82
	TINc	7.68	6.61	2.71	<i>1.58</i>	<b>0.84</b>	2.02	9	-
	TINr	3.15	2.73	1.04	1.19	<b>0.7</b>	<i>0.73</i>	7.6	-
	LSUNc	23.23	20.77	8.75	3.2	<b>2.02</b>	5.78	<i>2.8</i>	3.2
	LSUNr	2.64	1.81	0.36	0.43	<b>0.3</b>	<i>0.32</i>	3.4	36.16
	SVHN	2.72	2.34	2.61	4.89	<i>2.11</i>	<b>2.09</b>	-	17.16
	MNIST	<b>0</b>	<b>0</b>	<b>0</b>	2.52	1.77	<b>0</b>	-	0.36
	KMNIST	0.99	0.43	<b>0</b>	2.2	1.83	<b>0</b>	-	0.33
	FMNIST	1.67	0.34	0.34	3.83	2.37	<i>0.15</i>	-	<b>0.11</b>
	DTD	22.02	19.04	8.66	7.94	<b>5.71</b>	<i>7.56</i>	-	56.03
STL10	76.52	76.3	49.44	<i>34.04</i>	<b>29.3</b>	46.85	-	84.39	
CIFAR100	84.57	82.83	68.06	<i>42.43</i>	<b>35.77</b>	63.28	-	-	
CIFAR100	iSun	22.05	22.88	<i>6.26</i>	22.58	8.44	<b>1.55</b>	-	81.47
	TINc	31.79	33.07	<i>9.98</i>	28.04	13.53	<b>4.51</b>	41.7	-
	TINr	20.46	21.32	<i>6.7</i>	23.41	10.85	<b>4.64</b>	47.2	-
	LSUNc	38.33	37.29	23.29	50.63	26.51	<b>9.15</b>	50.2	<i>17.02</i>
	LSUNr	25.3	25.95	<i>5.87</i>	20.77	7.53	<b>1.96</b>	43	81.22
	SVHN	3.34	<i>2.37</i>	4.11	26.09	12.68	<b>1.8</b>	-	63.73
	MNIST	<b>0</b>	<b>0</b>	<b>0</b>	12.19	3.97	<b>0</b>	-	57.7
	KMNIST	0.04	0.1	<b>0</b>	6.94	2.17	<b>0</b>	-	16.63
	FMNIST	7.11	6.67	<b>1.74</b>	8.38	2.52	<i>2.32</i>	-	4.56
	DTD	24.5	22.78	<i>15.07</i>	49.49	29.89	<b>2.42</b>	-	86.83
STL10	79.64	78.31	<i>53.21</i>	68.27	63.54	<b>11.51</b>	-	79.36	
CIFAR10	92.07	91.11	86.75	87.47	<i>85.73</i>	<b>80.35</b>	-	-	

Table 2: OOD detection comparison against state-of-the-art OOD detectors. Comparison metric is FPR95, lower is better. **Best** results for a data set are shown in **blue and bold**, *second* best results are shown in *green and italics*. A dagger<sup>†</sup> is used when HDFF is ensemble; there are always 5 models in the ensemble. A double dagger<sup>‡</sup> is used to distinguish methods that are trained with the 1D Subs [57] training methodology. We see comparable performance for each method to the results from the main submission.

**Gram Matrices** Rather than measuring similarities between features, as we do in HDFF, Gram [49] in essence puts minimum and maximum thresholds between *correlations* of features. This is an important clarification as: i) Similarity between features (HDFF) is not the same as similarity between feature *correlations* of individual images and ii) Linking feature correlations back to visual similarity is not necessarily clear. Utilising defined ranges of feature correlations would necessarily allow inputs with approximately the same features as the training set to be given low deviations scores, allowing for *some* images to be interpreted as very visually similar. However, due to the injective matrix multiplication function used to compute the gram matrices, inputs with very different features to the training data can produce the same or similar feature correlations. This means that the interpretation of visual similarity can only be applied when we assume that features for new inputs are approximately similar to the training set, an assumption which is incompatible with the OOD task. An interpretation that can be used only *some* of the time is a difficult or nearly

ID set	OOD set	HDFF (Ours)	HDFF† (Ours)	Gram [49]	HDFF‡ (Ours)	HDFF†‡ (Ours)	Gram‡ [49]	Spectral‡ [57]
CIFAR10	iSun	4.1	3.86	1.79	1.79	<i>1.38</i>	<b>1.37</b>	-
	TINc	5.82	5.45	3.46	<i>2.8</i>	<b>2.31</b>	2.95	6.8
	TINr	4.03	3.81	2.09	2.4	<i>1.92</i>	<b>1.61</b>	6.2
	LSUNc	10.28	9.73	6.69	4	<b>3.16</b>	5.28	<i>3.7</i>
	LSUNr	3.76	3.73	1.23	1.74	<i>1.21</i>	<b>0.99</b>	3.8
	SVHN	3.73	3.52	3.57	4.86	<i>3.32</i>	<b>3.15</b>	-
	MNIST	1.42	1.14	<i>0.11</i>	3.72	3.36	<b>0.09</b>	-
	KMNIST	2.9	2.61	<i>0.26</i>	3.56	3.4	<b>0.17</b>	-
	FMNIST	3.25	2.47	<i>1.61</i>	4.37	3.66	<b>1.14</b>	-
	DTD	10.38	9.76	6.7	<i>6.11</i>	<b>5.29</b>	6.23	-
	STL10	23.46	24.03	19.42	<i>13.64</i>	<b>11.99</b>	20.26	-
CIFAR100	30	29.88	28	<b>5.63</b>	<i>13.3</i>	27.95	-	
CIFAR100	iSun	10.84	10.96	<i>5.03</i>	13.54	6.57	<b>2.46</b>	-
	TINc	13.68	13.62	<i>6.37</i>	15.22	9.03	<b>4.4</b>	18.9
	TINr	10.4	10.59	<i>5.42</i>	13.99	7.85	<b>4.5</b>	14.2
	LSUNc	16.59	15.7	<i>11.21</i>	17.95	12.91	<b>6.85</b>	13.9
	LSUNr	11.4	11.41	<i>4.86</i>	12.71	6.11	<b>2.54</b>	11.3
	SVHN	4.09	3.46	<i>4.32</i>	15.34	8.74	<b>2.92</b>	-
	MNIST	0.7	<i>0.11</i>	0.63	7.58	3.27	<b>0.01</b>	-
	KMNIST	1.47	1.56	<i>0.32</i>	4.93	2.46	<b>0.16</b>	-
	FMNIST	5.11	4.95	2.99	5.68	<i>2.94</i>	<b>2.7</b>	-
	DTD	11.8	10.93	<i>8.21</i>	22.08	15.74	<b>7.29</b>	-
	STL10	26.17	24.71	17.96	17.99	<i>15.27</i>	<b>6.13</b>	-
CIFAR100	36.87	35.15	32.8	26.71	<b>24.22</b>	<i>25.36</i>	-	

Table 3: OOD detection comparison against state-of-the-art OOD detectors. Comparison metric is Detection Error, lower is better. **Best** results for a data set are shown in **blue and bold**, *second* best results are shown in *green and italics*. A dagger† is used when HDFF is ensemble; there are always 5 models in the ensemble. A double dagger‡ is used to distinguish methods that are trained with the 1D Subs [57] training methodology. We see comparable performance for each method to the results from the main submission.

unusable interpretation at all, for this reason we do not consider Gram [49] to be interpretable in the same way as HDFF.

Figure 6 displays near-OOD images from CIFAR100 classified as the CIFAR10 truck class by Gram [49] with a deviation score lower than 2. Considering that the deviation score is unbounded with respect to how large it can be, choosing a threshold of 2 restricts the samples to those with no, or very little, deviations in feature correlations. Since Gram matrices do not always separate samples based on visual similarity, we see a number of samples outlined in red, from houses to electronic appliances, that do not fall under what would be expected to be similar to a truck. Images in orange are separated as questionably similar to the truck class, sharing some expected features (e.g wheels) with the truck class. In the interests of fairness we note that, consistent with our

		ResNet34		DenseNet3	
		HDFF	Gram	HDFF	Gram
CIFAR10	iSun	98.1	<b>99.8</b>	95	<b>99.8</b>
	TINc	97.6	<i>99.2</i>	97.2	<b>99.3</b>
	TINr	97.6	<b>99.7</b>	95.7	<b>99.7</b>
	LSUNc	98.7	<b>97.8</b>	95.7	<i>97.5</i>
	LSUNr	97.8	<b>99.9</b>	94.8	<b>99.9</b>
	SVHN	<b>99.6</b>	<i>99.5</i>	97.3	99.1
	MNIST	98.5	<i>99.97</i>	99.7	<b>99.99</b>
	KMNIST	97.7	<i>99.97</i>	99.6	<b>99.99</b>
	FMNIST	97.5	<i>99.9</i>	99.4	<b>99.92</b>
	DTD	<i>97.3</i>	<b>98</b>	92.4	97
	STL10	67.2	<b>87.2</b>	55.9	<i>82.6</i>
	CIFAR100	<b>88.2</b>	<i>79</i>	66.4	72
CIFAR100	iSun	86.9	<i>98.8</i>	95.5	<b>99</b>
	TINc	88.8	<b>97.7</b>	97.2	<b>97.7</b>
	TINr	87.7	<i>98.9</i>	95.5	<b>99</b>
	LSUNc	91.3	<i>92.1</i>	<b>93.4</b>	91.4
	LSUNr	85.4	<i>99.2</i>	95	<b>99.3</b>
	SVHN	96.9	96	<b>98.4</b>	<i>97.3</i>
	MNIST	87.9	<b>99.999</b>	99.96	<b>99.999</b>
	KMNIST	91.6	<b>99.998</b>	99.9	<i>99.996</i>
	FMNIST	94.3	<b>99.9</b>	99.7	<b>99.9</b>
	DTD	92.7	<b>97.3</b>	88.9	<i>94.2</i>
	STL10	78.9	<b>89</b>	53.2	<i>87.2</i>
	CIFAR10	<b>77</b>	<i>67.9</i>	49.5	64.2

Table 4: OOD detection comparison against state-of-the-art OOD detectors. Comparison metric is AUROC, higher is better. **Best** results for a data set are shown in **blue and bold**, *second* best results are shown in *green and italics*. All models are trained using cross-entropy loss. We notice that the performance of HDFF on DenseNet excels in far-OOD tasks but fails in near-OOD tasks, suggesting different network architectures are more sensitive to differing types of OOD data.

description in the paragraph above, visually similar objects, such as trains or buses, are present and form the majority of the low-deviation near-OOD samples. Importantly, we note that the visually dissimilar images with the red and orange borders in Figure 6, do not appear within the 15 degree visual similarity threshold whilst all the visually similar images with green borders do.

**MOOD & Spectral Discrepancy** Both MOOD [29] and Spectral Discrepancy [57] make no arguments for interpretability and analogues between their methods and HDFF cannot be drawn immediately. However, we do note that the notion of separating OOD samples based on a measure of complexity as proposed in [29] can be understood as a naive form of interpretability, though this aspect is unexplored in their work.

**DDU** Fundamentally, DDU [36] proposes a new uncertainty estimation method with applications in OOD detection as well as active learning. Methods falling

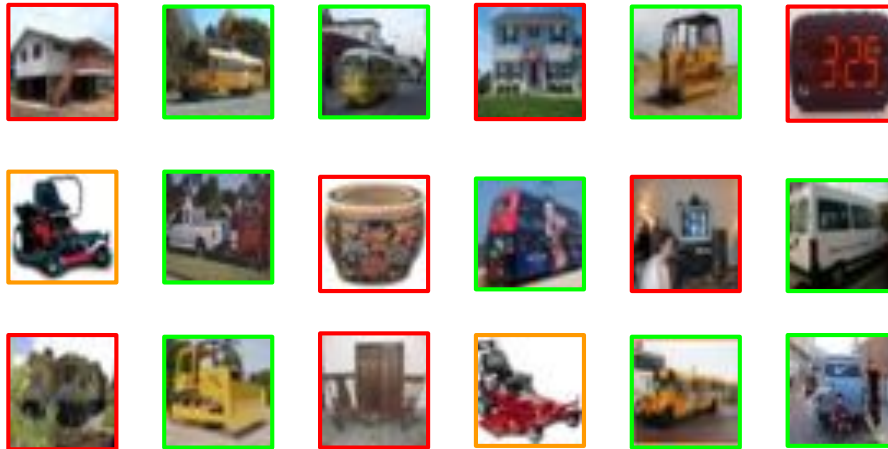


Fig. 6: Sample of CIFAR100 near-OOD images classified as the CIFAR10 ID truck class with a Gram [49] deviation score of less than 2 on the 1D Subspaces trained model. Images with **green** borders are visually and semantically similar to the ID truck class. Images with **red** borders are visually and/or semantically dissimilar to the ID truck class. Images with **orange** borders have some visual similarity to the truck class. Frequencies of green, red and orange images are not to scale, green images are more frequent.

under the banner of uncertainty estimation, like DDU, have their outputs interpreted as probabilities that the model has made an error. DDU [36] obfuscates this by considering the density of new samples in a high-dimensional Gaussian Mixture Model. Since densities in high-dimensional spaces can be arbitrarily low, interpreting the output of this density estimator is unintuitive (e.g. what does a density of  $10^{-6}$  signify for an input?).

## B.2 Inter-Sample Similarity

To our knowledge, we are the first work to allow for the comparisons of similarity between input samples, lending HDFF further to the interpretation of visual similarity. By comparing the descriptor vectors between two images, HDFF provides a quantitative metric that evaluates how visually similar the two input samples are. Importantly, since the angles between vectors is bounded between  $[0, 90]$  degree we can assign semantic meaning to these bounds with 0 corresponding to exactly matching images and 90 corresponding to images with no similarity at all. Figure 7 demonstrates a few examples of this, visualising the angular difference between images sampled from the CIFAR10 ID set.



Fig. 7: Visualisation of similarity between CIFAR10 ID samples using a 1D Subspaces trained WideResNet. Lines with angles between images corresponds to the angular distance between each images respective image descriptor vector. Comparisons are only made between direct neighbours to avoid clutter.

### B.3 Class Feature Similarity

Since HDFS is able to measure similarity of features from individual inputs as well between inputs and class descriptor vectors, it stands to reason that the similarity of the class descriptor vectors will say something about the features that consistently appear in a class. Figure 8 displays two heatmaps measuring the cosine similarity between the class descriptor vectors for two cross-entropy networks; WideResNet 8a and DenseNet 8b. An interesting observation is that the classes corresponding to vehicles ([0, 1, 8, 9] or [airplane, automobile, ship, truck] respectively) are more similar to each other than to the other classes. Additionally, all of the animal classes ([2, 3, 4, 5, 6, 7] or [bird, cat, deer, dog, frog, horse] respectively) are more similar to each other than to the vehicle classes. This detail indicates that a set of common features exists for these described vehicle and animal super classes. We note that the signal from this experiment is weak but still describes an interesting phenomena. We are intrigued at the implications of this result; future works could investigate isolating the unique features per class for greater OOD detection or even classification performance using the bundles.

## C Additional Ablations

### C.1 Computational Efficiency

HDC techniques are commonly used for computation or learning in low-power situations [35,19] and as such, we expect HDFS to introduce minimal computational overhead. For a full pass of the CIFAR10 test set, HDFS takes  $7.0 \pm 0.9$ s

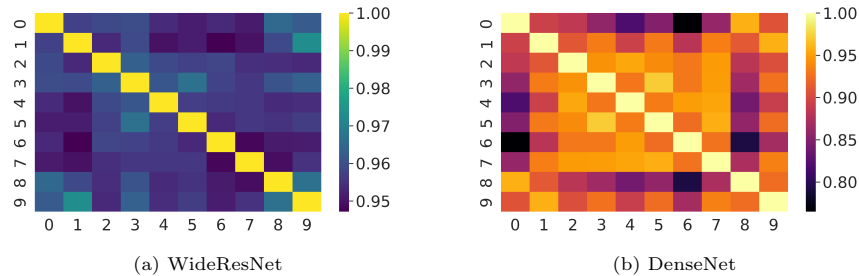


Fig. 8: Similarity heatmaps of class descriptor vectors calibrated from the CIFAR10 training set using cross-entropy trained WideResNet (a) and DenseNet (b). Heat scale corresponds to cosine similarity of feature bundle. Different colour maps are used to distinguish base models and avoid confusion on heat scale. Across both networks, although slightly more prevalent in (b) on the DenseNet architecture, a signal can be observed dividing the classes into two sets,  $[0, 1, 8, 9]$  and  $[2, 3, 4, 5, 6, 7]$ , with higher pair-wise similarity for classes contained within the same set. The separation of these sets indicates HDFF is separating based on visual similarity as  $[0, 1, 8, 9]$  (airplane, automobile, ship and truck respectively) all belong to vehicle-like classes and  $[2, 3, 4, 5, 6, 7]$  (bird, cat, deer, dog, frog and horse respectively) all belong to animal-like classes.

compared to a standard inference pass at  $6.0 \pm 0.7s$ , averaged over 5 independent runs. We note that this  $\approx 17\%$  increase is comparatively minor considering the near state-of-the-art performance that HDFF provides. By comparison, the closest equivalent method to ours, Gram [49] takes  $31.4 \pm 0.3s$  to complete a full inference pass over the CIFAR10 test set, meaning HDFF is much faster. Effectively, that it is more meaningful to compare the 5-ensemble of HDFF to Gram where the execution times would be more comparable. In this evaluation setting we see that there is no clear winner between HDFF and Gram; with HDFF performing better overall in the CIFAR10 settings and Gram performing better in the CIFAR100 settings. Additionally, we expect the computational efficiency of Gram to drop on larger networks due to the gram matrices scaling  $O(n^2)$  in computation and memory requirements with the number of channels. We further note that HDFF with only a single inference pass competes with or exceeds the Spectral Discrepancy detector [57] that requires 50 MC samples to be collected, necessitating a minimum increase of 5000%.

## C.2 Additional Layer Ablations

Figure 9 provides additional ablations of individual layer performance with respect to the other standard metrics for the benchmark defined in [28]; those being FPR@95, Detection Error and Maximum F1 Score. We make use of the same 12 BasicBlock hooks as in the main paper. Across both settings we see that the cropped datasets nearly perfectly mirror each other, indicating that there is a set of features that HDFF is consistently strong at detecting. In the CIFAR10 setting we see that across all metrics, there is no individual layer that performs

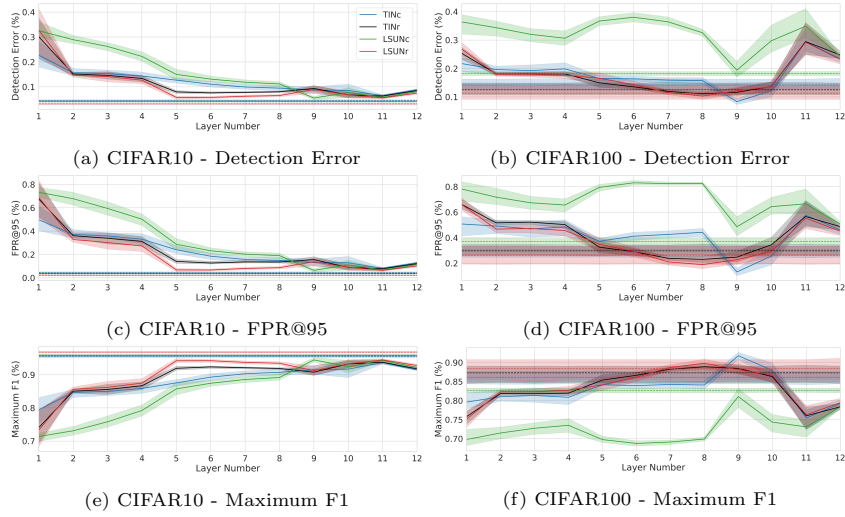


Fig. 9: Layer-wise ablation across multiple metrics for the 1D Subspaces trained model. We plot mean and 95% confidence interval for each datasets with the dotted lines corresponding to the performance of the fusion of feature maps across the network. For the CIFAR10 setting in (a), (c) and (e) it is clear that the fusion of feature maps from across the network provide the best performance. For the CIFAR100 setting in (b), (d) and (f) we see that violations of this characteristic are present in the later layers of 7, 8 and 9. Although some individual layers violate this characteristic, we note that no individual layer performs well across all of the OOD datasets.

at or above the level of the the fusion of feature maps. This trend is violated by the later layers, 7 through to 9 in the CIFAR100 setting. In particular, we see that the metrics that measure binarised performance, F1 and FPR@95, appear to have the largest increase above the fusion of features, usually in only a single layer. Overall, we make the same observation as in the main paper; there is no individual layer that performs well across all OOD datasets, assuming we already have the prior knowledge of how well each layer performs at this task. Future work into weighting individual layers based on predicted performance may be an important consideration.

### C.3 Preprocessing

In order to apply our hyperdimensional feature fusion to the feature maps of a DNN we first implemented a preprocessing pipeline that made use of a global pooling operation and mean-centering. Table 5 ablates these components on a subset of datasets with the AUROC metric, showing their influence to the overall results described in the main paper.

Table 5 offers us two core findings; firstly, mean-centering provides performance increases in every scenario, although in the max pooling CIFAR10 setting, these improvements are minute. Secondly, max pooling increases performance in

the CIFAR10 settings and average pooling provides better results on the whole for the CIFAR100 setting. We additionally note that the performance gaps between max and average pooling are relatively minor, with only LSUNc in the CIFAR100 setting having a discrepancy greater than 1%. Overall, both max and average pooling are approximately balanced with no clear better choice, whilst the addition of mean-centering always improves performance.

ID set	OOD set	Centering	Avg Pool	Max Pool
CIFAR10	TINc	✓	99.3	<b>99.7</b>
		✗	98.7	<b>99.7</b>
	TINr	✓	99.4	<b>99.7</b>
		✗	99.3	<b>99.7</b>
LSUNc	✓	99.3	<b>99.1</b>	
	✗	98.9	<b>99.1</b>	
LSUNr	✓	99.7	<b>99.9</b>	
	✗	99.5	<b>99.9</b>	
CIFAR100	TINc	✓	<b>94.4</b>	93.7
		✗	91.6	93.5
	TINr	✓	<b>95.1</b>	94.1
		✗	94.8	94.0
	LSUNc	✓	90.4	<b>91.8</b>
		✗	86.8	90.3
	LSUNr	✓	<b>95.9</b>	95.1
		✗	95.0	95.7

Table 5: Ablation of our feature preprocessing in terms of the AUROC metric in the single-inference pass setting with the 1D Subspaces trained model. **Best** result per ID + OOD dataset combination is coloured. Differing pooling operations provide better results dependant on the ID dataset, whereas mean-centering always improves performance.

## References

1. Bevanđić, P., Krešo, I., Oršić, M., Šegvić, S.: Simultaneous semantic segmentation and outlier detection in presence of domain shift. In: Pattern Recognition. pp. 33–47 (2019)
2. Blum, H., Sarlin, P.E., Nieto, J., Siegwart, R., Cadena, C.: The fishyscapes benchmark: Measuring blind spots in semantic segmentation. International Journal of Computer Vision **129**(11), 3119–3135 (2021)
3. Cimpoi, M., Maji, S., Kokkinos, I., Mohamed, S., Vedaldi, A.: Describing textures in the wild. In: Proceedings of the IEEE Conf. on Computer Vision and Pattern Recognition (CVPR) (2014)
4. Clanuwat, T., Bober-Irizar, M., Kitamoto, A., Lamb, A., Yamamoto, K., Ha, D.: Deep learning for classical japanese literature. CoRR **abs/1812.01718** (2018), <http://arxiv.org/abs/1812.01718>

5. Coates, A., Lee, H., Ng, A.Y.: An analysis of single layer networks in unsupervised feature learning. In: AISTATS (2011)
6. Deng, J., Dong, W., Socher, R., Li, L.J., Li, K., Fei-Fei, L.: Imagenet: A large-scale hierarchical image database. In: IEEE Conference on Computer Vision and Pattern Recognition. pp. 248–255 (2009)
7. Deng, L.: The mnist database of handwritten digit images for machine learning research. *IEEE Signal Processing Magazine* **29**(6), 141–142 (2012)
8. DeVries, T., Taylor, G.W.: Learning confidence for out-of-distribution detection in neural networks. arXiv preprint arXiv:1802.04865 (2018)
9. Di Biase, G., Blum, H., Siegart, R., Cadena, C.: Pixel-wise anomaly detection in complex driving scenes. In: IEEE/CVF Conference on Computer Vision and Pattern Recognition. pp. 16918–16927 (2021)
10. Gal, Y., Ghahramani, Z.: Dropout as a Bayesian approximation: Representing model uncertainty in deep learning. In: International Conference on Machine Learning (2016)
11. Gallant, S.I., Okaywe, T.W.: Representing Objects, Relations, and Sequences. *Neural Computation* **25**(8), 2038–2078 (2013)
12. Gayler, R.: Multiplicative binding, representation operators & analogy. In: Advances in analogy research: Integr. of theory and data from the cogn., comp., and neural sciences (1998)
13. Ge, L., Parhi, K.K.: Classification using hyperdimensional computing: A review. *IEEE Circuits and Systems Magazine* **20**(2), 30–47 (2020)
14. Gosmann, J., Eliasmith, C.: Vector-derived transformation binding: An improved binding operation for deep symbol-like processing in neural networks. *Neural Computation* **31**(5), 849–869 (2019)
15. He, K., Zhang, X., Ren, S., Sun, J.: Deep residual learning for image recognition. arXiv preprint arXiv:1512.03385 (2015)
16. Hein, M., Andriushchenko, M., Bitterwolf, J.: Why ReLU networks yield high-confidence predictions far away from the training data and how to mitigate the problem. In: IEEE/CVF Conference on Computer Vision and Pattern Recognition. pp. 41–50 (2019)
17. Hendrycks, D., Basart, S., Mazeika, M., Mostajabi, M., Steinhardt, J., Song, D.: Scaling out-of-distribution detection for real-world settings. arXiv preprint arXiv:1911.11132 (2019)
18. Hendrycks, D., Gimpel, K.: A baseline for detecting misclassified and out-of-distribution examples in neural networks. In: International Conference on Learning Representations (2017)
19. Hernández-Cano, A., Zhuo, C., Yin, X., Imani, M.: Real-time and robust hyperdimensional classification. In: Great Lakes Symposium on VLSI. p. 397–402 (2021)
20. Huang, G., Liu, Z., van der Maaten, L., Weinberger, K.Q.: Densely connected convolutional networks. In: Proceedings of the IEEE Conference on Computer Vision and Pattern Recognition (2017)
21. Huang, H., Li, Z., Wang, L., Chen, S., Dong, B., Zhou, X.: Feature space singularity for out-of-distribution detection. In: Workshop on Artificial Intelligence Safety (2021)
22. Kanerva, P.: Hyperdimensional computing: An introduction to computing in distributed representation with high-dimensional random vectors. *Cognitive Computation* **1**(2), 139–159 (2009)
23. Komer, B., Stewart, T., Voelker, A., Eliasmith, C.: A neural representation of continuous space using fractional binding. In: CogSci. pp. 2038–2043 (2019)

24. Krizhevsky, A., Hinton, G.: Learning multiple layers of features from tiny images. Tech. rep., University of Toronto (2009)
25. Lakshminarayanan, B., Pritzel, A., Blundell, C.: Simple and scalable predictive uncertainty estimation using deep ensembles. In: *Advances in Neural Information Processing Systems* (2017)
26. Lee, K., Lee, H., Lee, K., Shin, J.: Training confidence-calibrated classifiers for detecting out-of-distribution samples. In: *International Conference on Learning Representations* (2018)
27. Lee, K., Lee, K., Lee, H., Shin, J.: A simple unified framework for detecting out-of-distribution samples and adversarial attacks. In: *Advances in Neural Information Processing Systems* (2018)
28. Liang, S., Li, Y., Srikant, R.: Enhancing the reliability of out-of-distribution image detection in neural networks. In: *International Conference on Learning Representations* (2018)
29. Lin, Z., Roy, S.D., Li, Y.: Mood: Multi-level out-of-distribution detection. In: *Proceedings of the IEEE/CVF Conference on Computer Vision and Pattern Recognition (CVPR)*. pp. 15313–15323 (June 2021)
30. Liu, W., Wang, X., Owens, J., Li, Y.: Energy-based out-of-distribution detection. In: *Advances in Neural Information Processing Systems* (2020)
31. Maddox, W.J., Izmailov, P., Garipov, T., Vetrov, D.P., Wilson, A.G.: A simple baseline for bayesian uncertainty in deep learning. In: *Advances in Neural Information Processing Systems* (2019)
32. Maddox, W.J., Izmailov, P., Garipov, T., Vetrov, D.P., Wilson, A.G.: A simple baseline for bayesian uncertainty in deep learning. In: *Advances in Neural Information Processing Systems*. pp. 13153–13164 (2019)
33. Miller, D., Sunderhauf, N., Milford, M., Dayoub, F.: Class anchor clustering: A loss for distance-based open set recognition. In: *IEEE/CVF Winter Conference on Applications of Computer Vision*. pp. 3570–3578 (2021)
34. Miller, D., Sünderhauf, N., Milford, M., Dayoub, F.: Uncertainty for identifying open-set errors in visual object detection. *IEEE Robotics and Automation Letters* **7**(1), 215–222 (2021)
35. Morris, J., Hao, Y., Fernando, R., Imani, M., Aksanli, B., Rosing, T.: Locality-based encoder and model quantization for efficient hyper-dimensional computing. *IEEE Transactions on Computer-Aided Design of Integrated Circuits and Systems* (2021), to appear
36. Mukhoti, J., Kirsch, A., van Amersfoort, J., Torr, P.H.S., Gal, Y.: Deep deterministic uncertainty: A simple baseline. arXiv preprint arXiv:2102.11582 (2022)
37. Netzer, Y., Wang, T., Coates, A., Bissacco, A., Wu, B., Andrew, N.: Reading digits in natural images with unsupervised feature learning. In: *NIPS Workshop on Deep Learning and Unsupervised Feature Learning* (2011)
38. Neubert, P., Schubert, S., Protzel, P.: An introduction to hyperdimensional computing for robotics. *Künstliche Intelligenz* **33**(4), 319–330 (2019)
39. Neubert, P., Schubert, S., Schlegel, K., Protzel, P.: Vector semantic representations as descriptors for visual place recognition. In: *Robotics: Science and Systems* (2021)
40. Oberdiek, P., Rottmann, M., Fink, G.A.: Detection and retrieval of out-of-distribution objects in semantic segmentation. In: *IEEE/CVF Conference on Computer Vision and Pattern Recognition Workshops*. pp. 1331–1340 (2020)
41. Papernot, N., McDaniel, P.D.: Deep k-nearest neighbors: Towards confident, interpretable and robust deep learning. arXiv preprint arXiv:1803.04765 (2018)

42. Plate, T.: A common framework for distributed representation schemes for compositional structure. In: *Connectionist Systems for Knowledge Representation and Deduction*. pp. 15–34 (1997)
43. Postels, J., Blum, H., Cadena, C., Siegart, R., Gool, L.V., Tombari, F.: Quantifying aleatoric and epistemic uncertainty using density estimation in latent space. arXiv preprint arXiv:2012.03082 (2020)
44. Rahimi, A., Kanerva, P., Rabaey, J.M.: A robust and energy-efficient classifier using brain-inspired hyperdimensional computing. In: *International Symposium on Low Power Electronics and Design*. p. 64–69 (2016)
45. Rahman, Q.M., Sünderhauf, N., Dayoub, F.: Online monitoring of object detection performance post-deployment. arXiv preprint arXiv:2011.07750 (2020)
46. Rahman, Q.M., Sünderhauf, N., Dayoub, F.: Did you miss the sign? A false negative alarm system for traffic sign detectors. In: *IEEE/RSJ International Conference on Intelligent Robots and Systems*. pp. 3748–3753 (2019)
47. Ren, J., Fort, S., Liu, J., Roy, A.G., Padhy, S., Lakshminarayanan, B.: A simple fix to mahalanobis distance for improving near-OOD detection. arXiv preprint arXiv:2106.09022 (2021)
48. Rosenfeld, A., Zemel, R.S., Tsotsos, J.K.: The elephant in the room. CoRR **abs/1808.03305** (2018), <http://arxiv.org/abs/1808.03305>
49. Sastry, C.S., Oore, S.: Detecting out-of-distribution examples with Gram matrices. In: III, H.D., Singh, A. (eds.) *Proceedings of the 37th International Conference on Machine Learning*. *Proceedings of Machine Learning Research*, vol. 119, pp. 8491–8501. PMLR (13–18 Jul 2020), <https://proceedings.mlr.press/v119/sastry20a.html>
50. Saxe, A.M., McClelland, J.L., Ganguli, S.: Exact solutions to the nonlinear dynamics of learning in deep linear neural networks. In: *International Conference on Learning Representations* (2014)
51. Schlegel, K., Neubert, P., Protzel, P.: A comparison of vector symbolic architectures. *Artificial Intelligence Review* pp. 1–33 (2021)
52. Smolensky, P.: Tensor product variable binding and the representation of symbolic structures in connectionist systems. *Artificial Intelligence* **46**(1), 159–216 (1990)
53. Sünderhauf, N., Brock, O., Scheirer, W., Hadsell, R., Fox, D., Leitner, J., Upcroft, B., Abbeel, P., Burgard, W., Milford, M., et al.: The limits and potentials of deep learning for robotics. *The International Journal of Robotics Research* **37**(4-5), 405–420 (2018)
54. Xiao, H., Rasul, K., Vollgraf, R.: Fashion-MNIST: a novel image dataset for benchmarking machine learning algorithms. arXiv preprint arXiv:1708.07747 (2017)
55. Yu, F., Zhang, Y., Song, S., Seff, A., Xiao, J.: LSUN: Construction of a large-scale image dataset using deep learning with humans in the loop. arXiv preprint arXiv:1506.03365 (2015)
56. Yu, Q., Aizawa, K.: Unsupervised out-of-distribution detection by maximum classifier discrepancy. In: *IEEE/CVF International Conference on Computer Vision*. pp. 9518–9526 (2019)
57. Zaeemzadeh, A., Bisagno, N., Sambugaro, Z., Conci, N., Rahnavard, N., Shah, M.: Out-of-distribution detection using union of 1-dimensional subspaces. In: *IEEE/CVF Conference on Computer Vision and Pattern Recognition (CVPR)*. pp. 9452–9461 (2021)
58. Zagoruyko, S., Komodakis, N.: Wide residual networks. In: *British Machine Vision Conference*. pp. 87.1–87.12 (2016)

59. Zimek, A., Schubert, E., Kriegel, H.P.: A survey on unsupervised outlier detection in high-dimensional numerical data. *Statistical Analysis and Data Mining* **5**(5), 363–387 (2012)